JOURNAL OF COMPUTATIONAL PHYSICS 95, 85–100 (1991)

Computation of Sharp Phase Boundaries by Spreading: The Planar and Spherically Symmetric Cases*

G. CAGINALP AND E. A. SOCOLOVSKY

Mathematics Department, University of Pittsburgh, Pittsburgh, Pennsylvania 15260

Received July 24, 1989; revised April 20, 1990

The sharp interface that arises from any of the major transition problems (classical or modified Stefan, etc.) can be smoothed using the phase field approach as a numerical tool. The basic idea is that the thickness of the interface can be regarded as a mathematical free parameter which can be stretched beyond its physical value for computational convenience. The computations in one dimensional space and n dimensions with radial symmetry indicate that this is an efficient method for dealing with stiff equations and results in a very accurate interface determination without explicit tracking. The question of optimizing the interfacial thickness with respect to grid size is also considered empirically. The technique also provides a numerical verification of the concept of an unstable critical radius of solidification.

I. INTRODUCTION

The problem of numerical computation of a moving boundary has been of interest in many contexts (see [1] for a recent survey). In this paper we focus our attention mainly on (sharp) free boundaries which arise from phase transitions. Using the phase field model (see [2] and references contained therein) as a tool for approximating these problems, we demonstrate that the sharp interface can be spread dramatically without significant error. In a test case for which an analytical solution is available a computed phase field interface easily approximates the exact one to within three to four digits. These results are the computational aspect of the theory which was introduced in Section 4 of [3].

The (sharp interface) free boundary problems can be described as follows. For a region $\Omega \subset \mathbb{R}^n$ and $t \in \mathbb{R}^+$ the problem is to determine a function $u(x, t)$ and a surface $\Gamma(t) \subset \Omega$ such that the following are satisfied:

$$u_t = K \Delta u \qquad \text{in} \quad \Omega \backslash \Gamma(t), \tag{1.1}$$

$$lv = -K[\nabla u]^{+}_{-} \qquad \text{on} \quad \Gamma(t), \tag{1.2}$$

$$u = -\frac{\sigma}{\Delta s}\kappa - \alpha \frac{\sigma}{\Delta s} v \qquad \text{on} \quad \Gamma(t). \tag{1.3}$$

* Supported by NSF Grant DMS-8806909.

0021-9991/91 $3.00

Here l is the latent heat, K the diffusivity, κ the sum of principal curvatures at a point on the interface, σ the interfacial (or surface) tension, and α is a constant related to a relaxation time, all in dimensionless units. Also, $[\nabla u]^{+}_{-}$ is the jump in the gradient of u across Γ and v is the signed magnitude of the normal velocity (positive if the direction is $-$ to $+$, i.e., solidification). The quantity Δs is the entropy difference between the phases, and will be equal to 4 within the normalization we use.

The classical Stefan model [4] is given by (1.1)–(1.3) if the surface tension, σ, is zero. In recent years two modifications of this model have been studied [4] in an attempt to incorporate the effects of surface tension and dynamical undercooling. These are implemented by including nonzero σ and $\alpha\sigma$ terms, respectively, in (1.3). The problem of numerically solving (1.1)–(1.3) is especially difficult because of the need to compute the curvature of the interface. One of the early attempts to compute such a model used front tracking [5] which has been developed extensively in recent years for a variety of sharp interface problems (see e.g. [13]).

An alternative approach to phase boundary problems based on the concept of an order parameter, φ, and Landau–Ginzburg ideas, is the phase field equations. In their simplest form these may be expressed as

$$u_t + \frac{l}{2}\varphi_t = K\Delta u \tag{1.4}$$

$$\alpha\xi^2\varphi_t = \xi^2\Delta\varphi + \frac{1}{2a}(\varphi - \varphi^3) + 2u, \tag{1.5}$$

where ξ and a are parameters related to the microscopic physics and provide length scales. The macroscopic significance is in terms of the interfacial tension and thickness, as discussed below. These equations are subject to initial and boundary conditions such as

$$u(0, t) = u_0(x), \qquad \varphi(0, t) = \varphi_0(x), \qquad x \in \Omega, \tag{1.6}$$

$$u(x, t) = u_\partial(x), \qquad \varphi(x, t) = \varphi_\partial(x), \qquad x \in \partial\Omega,\ t > 0 \tag{1.7}$$

Under suitable conditions there exists a smooth solution [6] to the system (1.4)–(1.7). The interface in the equations is not defined by any discontinuity but as the set of points given by

$$\Gamma(t) \equiv \{x \in \Omega: \varphi(x, t) = 0\}. \tag{1.8}$$

The liquid and solid regions of Ω are then defined as regions of positive and negative φ, respectively. The boundary conditions (1.7) are to be chosen so that $\varphi = \varphi_\pm$ on $\partial\Omega$, where φ_+, φ_- are the largest and smallest roots of

$$f(u, \varphi) \equiv (2a)^{-1}(\varphi - \varphi^3) + 2u = 0. \tag{1.9}$$

The relationship between the phase field equations (1.4), (1.5) and the Stefan-type equations (1.1)–(1.3) has been described in [2, 3] as a consequence of the scaling relations between ξ, a, and α. In particular, the surface tension, σ, and the interfacial thickness, ε, are related by

$$\sigma = \frac{2}{3}\frac{\varepsilon}{a} = \frac{2}{3}\xi a^{-1/2}, \qquad \varepsilon = \xi a^{1/2}. \tag{1.10}$$

The distinct models given by (1.1)–(1.3) are then obtained by allowing $\varepsilon \to 0$ in each case but taking $\sigma \to 0$ only for the classical Stefan model, while σ remains fixed for the modified problem.

In this paper we adopt the perspective that the equations (1.4), (1.5) are a means of approximating, with a smooth interface, any of the sharp interface problems (1.1)–(1.3). The numerical results confirm that, using this approach, the interface can be spread significantly with a small relative change of its behaviour. For instance, an increase of about one order of magnitude in the interface width reduces the computation time by more than two orders of magnitude with little or no loss of accuracy, as we discuss later. The numerical experiments are for both one-dimensional problems and for radially symmetric annular problems in n-dimensional space.

The key idea applied in our computation is that the interfacial thickness, ε, can be varied over a broad range without significant change, *provided* that σ and α are close to the values of interest. The results can be appreciated from a physical point of view by considering how (1.4)–(1.5) differs from (1.1)–(1.3) if σ and α are the same in both systems. The basic physical difference is that the latent heat in (1.1)–(1.3) is released on a set of measure zero while it is released on a set of thickness ε in (1.4)–(1.5). The similarities are, of course, that the same amount of latent heat is released and the temperature at the interface is identical in both problems. Thus the hope of using this type of approximation rests on the ansatz that similarities are crucial while the differences are minimal. In fact, the release of latent heat over a thickness ε simply assists the diffusion of heat in the interfacial region which removes, only slightly more quickly, the only obstacle to further solidification. This means that the difference between the two models in noncritical situations should amount to a slight change in the diffusion constant.

We test and confirm these ideas in essentially four ways: (1) We approximate typical melting and freezing problems in the one-dimensional classical Stefan problem for which one can write an exact solution. In this case the computed solution attains a precision of three to four digits at a small to moderate expense. (2) The modified Stefan problem ($\sigma \neq 0$) is considered in an annular spherically symmetric domain in $\mathbb{R}^n$. Varying ε over a wide range, but such that it does not create extreme computational demands, we find that the interfacial behavior does not change significantly provided σ remains fixed throughout the scaling. (3) Again, with $\sigma \neq 0$, we consider the sensitivity of the procedure in a delicate problem of unstable equilibrium of a solid sphere (at critical radius), surrounded by its melt.

We find a numerical verification of this instability by slightly perturbing σ and the initial location of the interface. A much larger change in ε does not appreciably alter the development of the interface. (4) In the one-dimensional modified Stefan problem ($\sigma \neq 0$, $\alpha \neq 0$) the curvature is trivially zero, so that the role of the dynamical undercooling term $-\alpha\sigma v$ in (1.3) can be tested independently. We demonstrate numerically that this converges to the classical Stefan case if and only if $\alpha\sigma$ approaches zero.

The intrinsic limitation of our method also involves the size of ε. If the geometry is very complex, e.g., in computing side-branching in dendritics, then ε must be small in comparison with the geometric scales in order to resolve the interface. Since we are using a uniform mesh, this means that the cost increases. However, such computations are lengthy with other methods as well. Furthermore, there is no reason an adaptive grid (using a finer mesh in the areas closer to the interface) cannot be used in conjunction with our methods.

To summarize briefly, the numerical calculations are corroborated by self-consistency, comparison with exact solutions, and known physical experiments. An announcement of part of this work has appeared in [7]. Other numerical work involving phase field equations without considering these limits includes [10, 11].

II. Initial and Boundary Conditions for Phase Field Equations and Numerical Procedures

The problems we consider in this paper are either one-dimensional or spherically symmetric. Hence we let r be the radial variable and $\Omega \subset \mathbb{R}^n$ be the annular region $0 < A \leqslant r \leqslant B$. The phase field equations [(1.4) (1.5)] can be written as

$$u_t = K\left[u_{rr} + \frac{(n-1)}{r}u_r\right] - \frac{l}{2\alpha}\left[\varphi_{rr} + \frac{(n-1)}{r}\varphi_r + (2a\xi^2)^{-1}(\varphi - \varphi^3) + 2\xi^{-2}u\right] \tag{2.1}$$

$$\varphi_t = \alpha^{-1}\left[\varphi_{rr} + \frac{(n-1)}{r}\varphi_r + (2a\xi^2)^{-1}(\varphi - \varphi^3) + 2\xi^{-2}u\right]. \tag{2.2}$$

Since we are adopting the perspective that these equations will be used as an approximation tool for the sharp interface problems (1.1)–(1.3), we need to consider the initial and (external) boundary conditions on the latter. The procedure we define below is a method for translating the initial and boundary conditions (1.1)–(1.3) into conditions on (1.4)–(1.5), i.e., (1.6) and (1.7). This method is quite general and is not restricted to the geometries of the calculations presented.

In order to distinguish between the two models, we let $u^{(s)}$ denote the solution to the sharp interface problems (1.1)–(1.3), while u, φ are solutions to (1.4)–(1.5). Since the φ variable is not in the problem (1.1)–(1.3), we let $\varphi^{(s)}$ be a tracking variable so that

$$\varphi^{(s)}(r, t) = \begin{cases} 1 & \text{if } r \text{ is in the liquid phase region} \\ -1 & \text{if } r \text{ is in the solid region.} \end{cases} \tag{2.3}$$

Note that in the classical Stefan model $\varphi^{(s)}$ can be defined simply as the sign of u.

The problems (1.1)–(1.3) are generally accompanied by initial condition $u^{(s)}(r, 0)$, which is continuous but may have a discontinuous gradient, and boundary conditions $u_{\partial}^{(s)}(r, t)$. Within our geometry, we can write

$$u_{\partial}^{(s)}(A, t) = u_A, \qquad u_{\partial}^{(s)}(B, t) = u_B(t). \tag{2.4}$$

The interface, which we denote by $\Gamma^{(s)}(t)$, belongs to $[A, B]$ and is prescribed at the initial time as the point r_0 at which $\varphi^{(s)}$ changes sign.

Given the initial and boundary conditions (2.3), (2.4) for the sharp interface problem we now *define* the choice of such conditions for the phase field equations (1.4)–(1.5) which are to approximate (1.1)–(1.3). At this stage, the values of ξ, a, α (and consequently σ, ε) have been set. We define $u(r, 0)$ as an appropriate mollification of $u^{(s)}(r, 0)$, so that the sharp discontinuity of the derivative of $u^{(s)}$ becomes a smooth transition occurring over a distance comparable to ε. In particular, we take

$$\begin{aligned} u_0(r) \equiv u(r, 0) = a_0 &+ \left(\frac{b_1 + b_2}{2}\right)(r - r_0) + \left(\frac{b_2 - b_1}{2}\right)(r - r_0)\,\psi\left(\frac{r - r_0}{\varepsilon}\right) \\ &+ \left(\frac{c_1 + c_2}{2}\right)(r - r_0)^2 + \left(\frac{c_2 - c_1}{2}\right)(r - r_0)^2\,\psi\left(\frac{r - r_0}{\varepsilon}\right) + \cdots, \end{aligned} \tag{2.5}$$

where r_0 is the initial location of the interface, and choose as smoothing function $\psi(s) = \tanh(5s)$. The coefficients in (2.5) are those of $u^{(s)}(r, 0)$ which has an expression identical to (2.5) but with $\psi(s) = 1$ for $s > 0$ and $\psi(s) = -1$ for $s < 0$. For consistency with (1.2)–(1.3), a_0 is required to be

$$a_0 \equiv -\frac{1}{4}\sigma\left[\frac{(n-1)}{r_0} + \alpha v\right]$$

with

$$v \equiv -\frac{K}{l}(b_2 - b_1) \equiv -\frac{K}{l}[\nabla u_0]^+.$$

Note that this is merely a requirement of internal consistency of the initial conditions for the *sharp* interface problem and does not constitute additional conditions on either model.

The smoothing of initial data is not essential for our method. One can use the initial conditions of the corresponding sharp interface problem directly without a very significant change in the computations. We have chosen to demonstrate the idea of smoothing of initial data because it transforms the original sharp interface problem into one which is entirely smooth. In some subtle problems in higher dimensions it is possible that this will make a substantial difference. The boundary conditions on u are then (to exponentially small error) identical to (2.4), so that

$$u_{\partial}(A, t) = u_A, \qquad u_{\partial}(B, t) = u_B(t). \tag{2.6}$$

The boundary conditions on φ are determined from (2.6) and (1.9); i.e.,

$$\varphi_{\partial}(A, t) = \varphi_A, \qquad \varphi_{\partial}(B, t) = \varphi_B(t), \tag{2.7}$$

where φ_A is the root of $f(u_A, \varphi_A) = 0$ closest to $\varphi^{(s)}(A, 0)$ and φ_B is the root of $f(u_B, \varphi_B) = 0$ near $\varphi^{(s)}(B, 0)$. Also using these values, we then construct the initial value $\varphi(r, 0)$ by means of the ad hoc formula

$$\varphi_0(r) \equiv \varphi(r, 0) = \begin{cases} \varphi_A, & A \leqslant r < r_1 \\ [\varphi(r_2, 0) - \varphi_A](r - r_1)/(r_2 - r_1) + \varphi_A, & r_1 \leqslant r < r_2 \\ \operatorname{sign}(\varphi_B) \tanh((r - r_0)/2\varepsilon), & r_2 \leqslant r \leqslant r_3 \\ [\varphi(r_3, 0) - \varphi_B](r - r_4)/(r_3 - r_4) + \varphi_B, & r_3 < r \leqslant r_4 \\ \varphi_B, & r_4 < r \leqslant B, \end{cases} \tag{2.8}$$

where r_0 is the initial location of the interface and

$$r_1 = \tfrac{3}{4}A + \tfrac{1}{4}r_0, \qquad r_2 = \tfrac{1}{2}(A + r_0), \qquad r_3 = \tfrac{1}{2}(B + r_0), \qquad r_4 = \tfrac{3}{4}B + \tfrac{1}{4}r_0.$$

Note that φ_0 is just a piecewise smooth approximation of $\varphi^{(s)}(r, 0)$ that makes the transition occur smoothly over a distance comparable to 10ε, plus an adjustment for the precise boundary conditions. In particular, the value of φ near the external boundaries $r = A$, B must be such that $f(u, \varphi) = 0$ so that the derivatives of φ are close to zero.

Our expectation is that the natural evolution of the phase field equation is captured by these regularizations of initial and boundary conditions, thereby improving the accuracy for the entire problem.

The computational procedure is as follows. First the sharp interface problem to be studied is fixed. Then entering ξ, a, and α the initial and boundary values for u and φ are calculated and Eqs. (1.4)–(1.5) are solved. To obtain more accurate results, it is only necessary to compute with smaller values of ξ and a, subject to the scaling of (1.10).

At this stage our principal objective is to validate our approach. The computations for Eqs. (1.4)–(1.5) were done with PDECOL, a general package to solve nonlinear PDEs that uses the method of lines with collocation in space, see [8]. We are studying more specific computational techniques for this problem, for example, an unconditionally stable scheme based on the semigroup approach of [9]. We shall report on these results elsewhere.

III. Approximating a Modified Stefan Model

A problem of considerable interest in phase boundaries is the sharp interface problem posed by (1.1)–(1.3) in which σ and α are nonzero. This problem, which is often part of a larger set of equations in a more complex system, is difficult to

study numerically because of the need to compute the curvature of the interface at all of the interface nodes for every time step. In this section we present results which demonstrate that (1.1)–(1.3) can be approximated by a diffuse interface via the phase field equations (1.4), (1.5) and the scaling relations (1.10). The parameters ξ and a must be adjusted so that σ is the given (fixed) value of surface tension. In principle, the interfacial thickness, ε, is a physical quantity which is often extremely small (in our dimensionless length scale). However, our key physical ansatz is that the value of ε can be changed drastically without significant change in the evolution of the interface, as discussed in Section 1. The situation for σ, however, is quite different, since even a small change in the surface tension generally results in a substantial change in the results (see Sections IV, V).

Given σ, from (1.10) ε and ξ are determined by choosing a. The limitations on a are given by two constraints. First the φ roots of (1.9) must have the proper qualitative behaviour, i.e., three distinct real roots which means that a cannot be large. Second, there must be enough points at the interface so that $\int (\varphi')^2\, dr$ can be determined accurately and remains constant in time, since it essentially is the surface tension. The limitation on the number of points and the stiffness of the equations imply that a is not too small. With a uniform mesh, empirically we found that the optimal mesh spacing Δr is such that ε is between $0.75\,\Delta r$ and $1.1\,\Delta r$.

Next, the initial and boundary conditions are determined following the procedure in Section 2. Given the initial conditions $u^{(s)}(r, 0)$, $\varphi^{(s)}(r, 0)$, and the boundary conditions (2.3)–(2.4), with (2.5)–(2.8), we obtain the associated initial and boundary

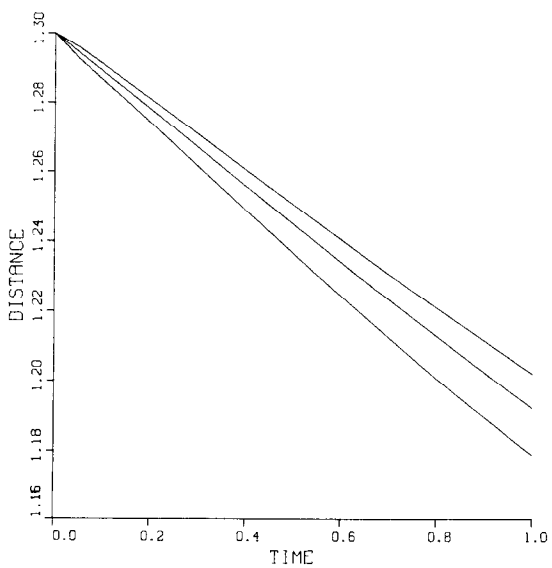

FIG. 1. Computed interfaces for the modified Stefan problem with $\sigma = 0.08533$. From top to bottom the curves correspond to $\varepsilon = 0.00128$, $\varepsilon = 0.02048$, and $\varepsilon = 0.04608$.

TABLE I

$\sigma = 0.085\hat{3}$

Experiment	a	ξ	ε	Total intervals	Ratio $\varepsilon/\Delta r$
1	0.36	0.0768	0.04608	80	3.6864
2	0.16	0.0512	0.02048	100	2.048
3	0.01	0.0128	0.00128	800	1.024

conditions u_0, φ_0, $u_{\hat{\rho}}$, $\varphi_{\hat{\rho}}$. Thus (1.4), (1.5), (2.5)–(2.8) can now be studied as a complete parabolic system.

We note that for each value of ε we obtain a different physical problem. Furthermore, for any nonzero ε Eq. (1.4), (1.5) differ physically from the sharp interface problems (1.1)–(1.3). The main difference is that the latent heat is released over an interface width of about 10ε. There is another difference in that the heat equation is only approximately valid in the solid and liquid regions. Our conjecture that neither of these is as important as ensuring the correct interfacial relation, (1.3), can be tested by varying ε in typical melting and freezing problems. In a prototype case, we take the three-dimensional annular region $1 \leqslant r \leqslant 2$, and assume that the interface is initially at $r = 1.3$ and that the initial conditions favor melting. We vary ε over a broad range and examine the differences in the evolution of the interface. Figure 1 illustrates the results.

For simplicity we took $K = l = \alpha = 1$ and only the first three terms of (2.5) were used with left slope $b_1 = 0.05$ and right slope $b_2 = 0.1$. The rest of the data is in Table I. The self-consistency evident in Fig. 1 confirms our ansatz. For larger values of ε, the interface is thicker and the latent heat is dissipated slightly more rapidly from the interface. However, this small change in the dissipation rate makes a minor difference in the latent heat balance (1.2) (which is implicitly part of the phase field equations) and even less for (1.3), since the temperature itself is likely to change very slightly due to the change in thickness. Thus, the main controlling mechanism for the growth of the interface, (1.3), is not significantly altered for different values of ε with σ held fixed (see Table I).

IV. Approximating the Classical Stefan Model—Comparison with Exact Solutions

The classical Stefan model is defined by (1.1)–(1.3) with $\sigma \equiv 0$. In the scaling limit $\sigma \to 0$, $\varepsilon \to 0$ (see (1.10)), the phase field equations (1.4)–(1.5) approach the classical Stefan model [3]. Physically, this means that both the surface tension and interfacial thickness approach zero. As discussed in Section I, the goal is to make σ as close to the actual value (zero in this case) while making ε no smaller than is practical for computation.

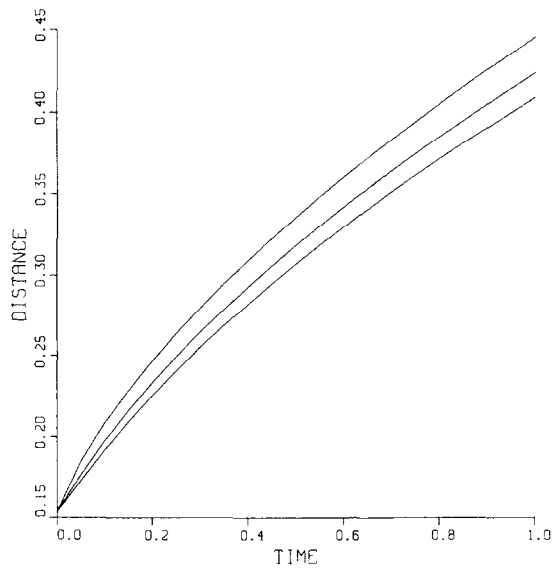

FIG. 2. Computed interfaces for the classical Stefan problem with $\sigma = 0.08533$. From top to bottom the curves correspond to $\varepsilon = 0.04608$, $\varepsilon = 0.2048$, and $\varepsilon = 0.00128$.

Given a set of initial and boundary conditions for the classical Stefan model, the corresponding set of conditions for (1.4)–(1.5) have been obtained in a slightly different way from that which is described in Section II. Instead of (2.5), the given initial condition for u is used. The absence of smoothing is compensated in part by the grid resolution and the condition that the piecewise polynomials used in the computations are at least C^1 at the gridpoints.

In Fig. 2 we again observe the self-consistency as we vary ε by a factor of 36. With the package and machine used in the computations, the CPU time changed by a factor of 560, mainly due to the increased stiffness of the equations.

The classical Stefan model offers the possibility of testing our ideas against exact solutions of the form

$$u^{(s)}(x, t) = \begin{cases} C_1[\operatorname{erf}(\beta/2) - \operatorname{erf}(r/2\sqrt{t+t_0})]\operatorname{erf}(\beta/2) & \text{if} \quad r \leqslant s(t),\ t \geqslant 0 \\ C_2[\operatorname{erf}(\beta/2) - \operatorname{erf}(r/2\sqrt{t+t_0})]/[1 - \operatorname{erf}(\beta/2)] & \text{if} \quad r > s(t),\ t \geqslant 0 \end{cases}$$

with interface

$$s(t) = \beta\sqrt{t+t_0}, \qquad t \geqslant 0,$$

where β is the solution of

$$\frac{2}{\sqrt{\pi}} e^{-\beta^2/4}[C_2/(1 - \operatorname{erf}(\beta/2)) - C_1/\operatorname{erf}(\beta/2)] - \beta = 0.$$

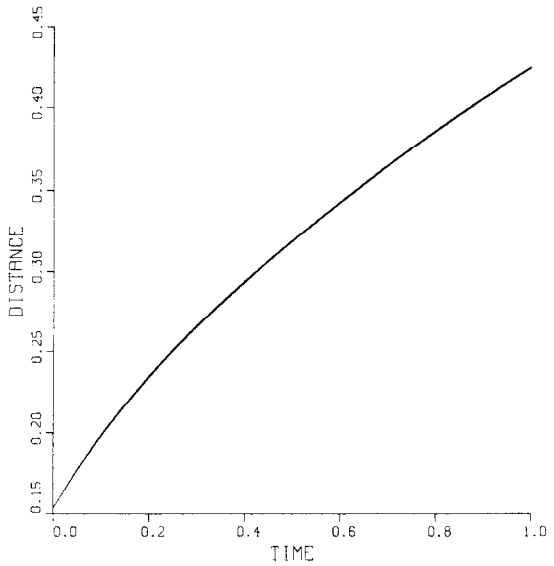

FIG. 3. Exact and computed interface for the classical Stefan problem with $\sigma = 0.00533$ and both $\varepsilon = 0.00512$ and $\varepsilon = 0.00128$.

For our computations we chose $A = 0$, $B = 1$, $C_1 = -0.085$, $C_2 = -0.015$, $\beta = 0.396618$, and $t_0 = 0.15$ so that our boundary conditions become

$$u(0, t) = C_1, \qquad u(1, t) = u^{(s)}(1, t)$$

$$\varphi(0, t) = \varphi_0(0), \qquad \varphi(1, t) = \frac{2}{\sqrt{3}} \cos\left(\frac{1}{3} \arccos(6\sqrt{3}\, au(1, t))\right).$$

The results displayed in Fig. 3 show excellent agreement in the location of the interface and correspond to experiments 1 and 4 of Table II. In Experiment 2 we increased the number of gridpoints and found the difference with the results of Experiment 1 to be negligible. This confirms that the accuracy of the approximation

TABLE II

$\sigma = 0.005\hat{3}$

Experiment	a	ξ	ε	Relative error for interface		Mesh intervals	
				Maximum	$t = 1$	Total	$\varepsilon/\Delta r$
1	0.64	0.0064	0.00512	0.003726	0.000823	200	1.024
2	0.64	0.0064	0.00512	0.003915	0.000817	500	2.56
3	0.32	0.0045255	0.00256	0.001936	0.001787	300	0.768
4	0.16	0.0032	0.00128	0.003113	0.003104	500	0.64
5	0.0625	0.002	0.0005	0.069093		1000	0.5

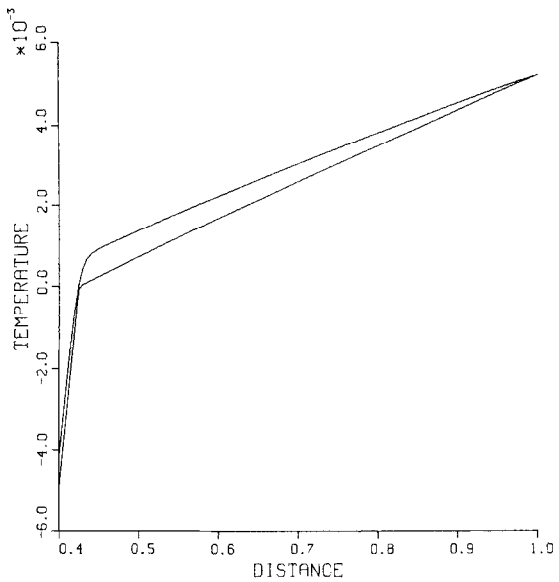

FIG. 4. Exact and computed solution for the classical Stefan problem with $\sigma = 00533$ and $\varepsilon = 0.00512$.

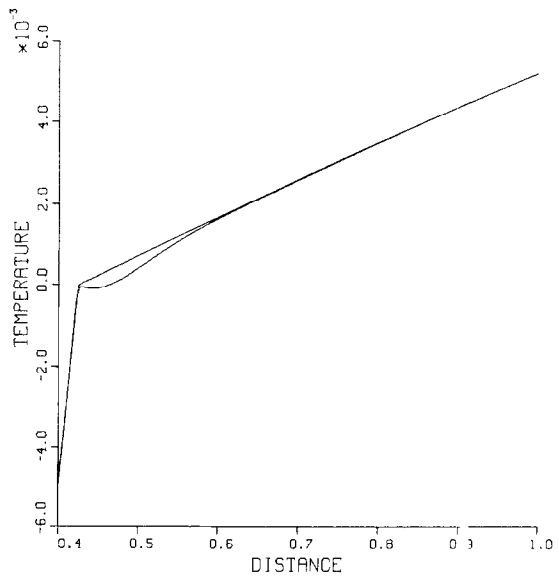

FIG. 5. Exact and computed solution for the classical Stefan problem with $\sigma = 0.00533$ and $\varepsilon = 0.00128$.

depends almost exclusively on σ and ε. In Experiments 3 and 4, ε is decreased, which insignificantly lessens the accuracy of the interface, but improves slightly the accuracy of the solution (u, φ). This is illustrated in Figs. 4 and 5, which correspond to Experiments 1 and 4, respectively. Decreasing ε further in Experiment 5, the increase in stiffness and low grid resolution destroys the accuracy of the computations before $t = 1$ is reached.

The one-dimensional problem also offers an opportunity to examine the influence of the kinetic undercooling term ($-\alpha\sigma v$ in (1.3)), since the curvature κ vanishes in this geometry. This effect is clearly observed in Fig. 5. Our experiments repeatedly confirm that σ is the parameter that determines the accuracy of the approximation, while the role of ε is secondary and should not be made unnecessarily small.

V. Optimizing Interfacial Thickness and Grid Size

We pursue the issue of selecting the interfacial thickness ε in the conjunction with the selection of mesh size Δr. Throughout our computations we have used uniform meshes. The rationale for this decision is that to use an adaptive grid requires either tracking the interface (at least approximately), or implementing some other criterion to determine where to concentrate gridpoints. Our objective is to choose ε and Δr that yield the most accurate results at a reasonable computational cost.

The physical problem specifies the value of the surface tension σ which by (1.10) satisfies $\sigma = \frac{2}{3}\varepsilon a^{-1}$. The constraint on a is that it is small enough so that (1.9) has three distinct real roots, which is their correct qualitative structure. As ε and a are made smaller the phase field equations approximate the sharp interface problems better. Essentially, the reasons are that the latent heat is released along a thinner region and that the heat equation is more accurately approximated away from the interface.

On the other hand, the surface tension is given (to first order) by

$$\sigma = \frac{\varepsilon}{a} \int_{-\infty}^{\infty} (\phi_\rho^0)^2 \, d\rho,$$

where ϕ^0 is the first-order inner solution to (1.5) in the inner or "stretched" variable $\rho = r/\varepsilon$, with r normal to the interface. An accurate evaluation of this quantity is essential from a physical point of view, hence it is necessary to have enough gridpoints on the interfacial region where φ makes its transition to determine its internal structure precisely. Furthermore, it is clear from (2.1)–(2.2) that the stiffness of the equation is proportional to ε^{-2}.

An optimal choice of ε and Δr is done by balancing the above competing factors. Our computationally verified conjecture is that a moderate stiffness and an adequate ratio for $(\varepsilon/\Delta r)$ are more important than taking ε very small. Physically the reason is that surface tension is more critical than how the latent heat is released or the precise validity of the heat equation away from the interface. We

have observed that if the grid resolution is too low, even for moderate values of ε, the results lose their accuracy. Also if ε is too small, even with a good ratio $\varepsilon/\Delta r$, the results do not improve and the computational cost is much higher due to the increased stiffness. For example, we repeated Experiment 5 of Table II with a ratio $\varepsilon/\Delta r = 1$ and time up to $t = 0.1$. The maximum relative error for the interface was 0.001873 as opposed to 0.001373 in Experiment 4 for the same time interval. The time interval is $\frac{1}{10}$ the time interval of Experiment 4, yet it required 1.17 times the CPU time of Experiment 4. Moreover, Experiment 4 required 8.59 times more CPU time than Experiment 2, and since the number of gridpoints is the same, this gives further evidence of the cost of increased stiffness. The most suitable value for the ratio $\varepsilon/\Delta r$ was determined empirically and we found that it is in the range $0.75 < \varepsilon/\Delta r < 1.1$.

VI. The Critical Radius Instability of Solidification

We now discuss a well-known instability in materials science. Our purpose is twofold. First, we provide computational justification for this instability. Second, we use this subtle problem to validate our approach. In particular, the numerical experiments verify that the interface thickness can be varied greatly even in this delicate problem without significant change in the interface motion.

The physical problem can be described as follows. A solid sphere is in equilibrium with its melt. Mathematically, this means that the sphere has as its sum of principal curvatures, κ_0, and both the solid and liquid are at constant temperature u_0 given by

$$u_0 = -\sigma_0 \kappa_0 / 4 \tag{5.1}$$

which is the Gibbs–Thomson relation for an interface in equilibrium. The velocity of the interface is zero in this case and clearly Eqs. (1.1)–(1.3) are satisfied. A hypothetical experiment shows, however, that this equilibrium is unstable [12]. Suppose the constants l and K are adjusted so that only a small amount of heat remains near the interface after solidification (i.e., l is small while K is large). If the sphere is perturbed to a slightly larger one (i.e., κ_0 is perturbed to κ_1 where $\kappa_1 < \kappa_0$) then (5.1) is no longer satisfied. If the physical problem is governed by (1.1)–(1.3) then (1.3) implies that

$$v = -(\Delta s u + \sigma \kappa)/\alpha\sigma > 0. \tag{5.2}$$

This means that further solidification will occur. If the system is subjected to Dirichlet boundary conditions and l, K^{-1} are small, then one expects that the material will continue to freeze until it is all solid. Note that perturbing σ to a smaller value will have the same effect, although this is a computational but not a physical perturbation, since surface tension is a property of the material. In the opposite direction, i.e., $\kappa_1 > \kappa_0$, one has complete melting in an analogus way. This instability is confirmed numerically as discussed below.

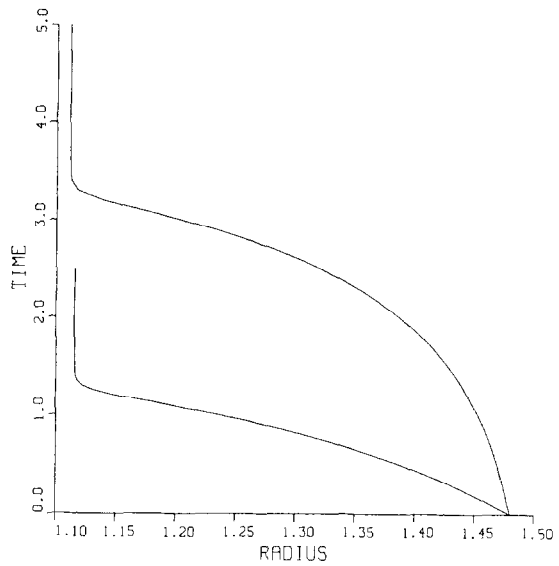

FIG. 6. Computed interfaces for critical radius instability. From top to bottom the curves correspond to $\sigma = 0.15$ and $\sigma = 0.16\hat{6}$.

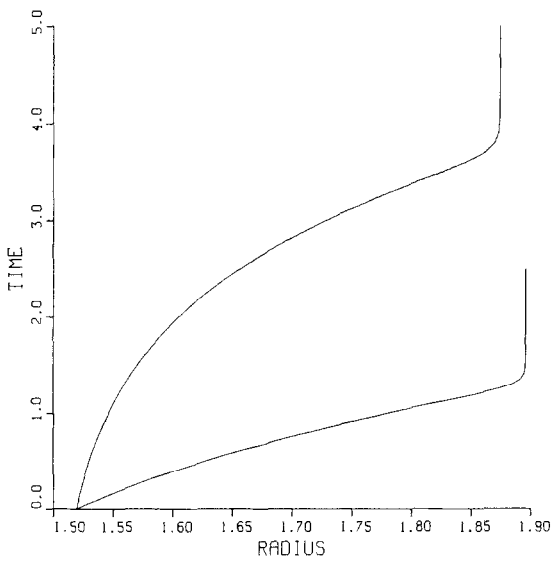

FIG. 7. Computed interfaces for critical radius instability. From top to bottom the curves correspond to $\sigma = 0.15$ and $\sigma = 0.13\hat{3}$.

TABLE III

Experiment	a	ζ	σ	Initial location of interface	ε	Ratio $\varepsilon/\Delta r$
1	0.16	0.09	0.15	1.48	0.036	7.2
2	0.16	0.1	$0.16\hat{6}$	1.48	0.04	8.0
3	0.16	0.09	0.15	1.52	0.036	7.2
4	0.16	0.08	$0.13\hat{3}$	1.52	0.032	6.4
5	0.16	0.09	0.15	1.5	0.036	7.2

The three-dimensional computational region is $1 \leqslant r \leqslant 2$, with $K = 10$, $l = 0.1$, and $\alpha = 1$. In (5.1) the curvature is $\kappa_0 = (n-1)/r_0$ and, by selecting the equilibrium position of the interface to be $r_0 = \frac{3}{2}$, we obtain $\kappa_0 = \frac{4}{3}$. We took $\sigma_0 = 0.15$; consequently, the equilibrium temperature is $u_0 = -0.05$. The results are illustrated in Figs. 6 and 7 and the rest of the relevant data is in Table III.

We note that in each of the cases above, the material melts or freezes completely (except for a transition layer near one of the boundaries). The reason for the transition layer is that our boundary conditions constrain it to be in a particular phase.

In order to obtain further numerical confirmation of the concept of a critical radius, we assume the values u_0, κ_0, σ, which are consistent with (5.1). In this case, theory implies that the interface be in unstable equilibrium. The equilibrium is most

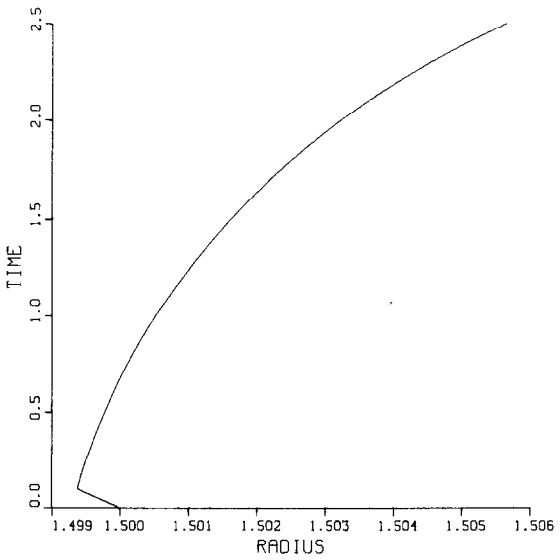

FIG. 8. Computed interface for critical radius instability. Unstable equilibrium at $r = 1.5$ for uniform temperature $u = -0.05$ and $\sigma = 0.15$.

delicate when l is small and K is large for reasons discussed above. Thus in Experiment 5 of Table III we compute with these parameters and initial conditions, and obtain the results shown in Fig. 8. The results imply that the unstable equilibrium is maintained for a much longer time period (compared to Figs. 6 and 7). Even when ε is changed by a factor of 10, one obtains approximately the same rate of departure from this unstable equilibrium. Thus a very small change in σ disturbs unstable equilibrium much more than a large change in ε.

These results provide the first computational confirmation, to the best of our knowledge, of the concept of a critical radius of solidification and the resulting instability within the symmetry group of the sphere. Moreover, these numerics demonstrate that the phase field methods are quite capable of describing the interface even in the most subtle situations. In particular the spreading of the interface is possible without sacrificing much accuracy in this critical problem.

REFERENCES

1. J. GLIMM, *Proceedings, of Nice Conference, Jan.* 1988.
2. G. CAGINALP, *Phys. Rev. A* **39**, 5887 (1989).
3. G. CAGINALP, in *Symposium on Material Instabilities in Continuum Mechanics*, Heriot-Watt University, edited by J. Ball (Oxford Univ. Press, London, 1988), p. 35.
4. A. BOSSAVIT, A. DAMLAMIAN, AND M. FREMOND (Eds.), in *Free Boundary Problems: Applications and Theory* (Pitman, Boston, 1985).
5. J. SMITH, *J. Comput. Phys.* **39**, 112 (1981).
6. G. CAGINALP, *Arch. Rat. Mech. Anal.* **92**, 205 (1986).
7. G. CAGINALP AND E. A. SOCOLOVSKY, *Appl. Math. Lett.* **2**, 117 (1989).
8. N. K. MADSEN AND R. F. SINCOVEC, *ACM Trans. Math. Software* **3**, No. 5, 326 (1979).
9. E. A. SOCOLOVSKY, *Math. Comput.* **47**, 411 (1986).
10. J. LIN AND G. FIX, *Theory Methods Appl.* **12**, 811 (1988).
11. G. CAGINALP AND J. LIN, *IMA J. Appl. Math.* **39**, 51 (1987).
12. B. CHALMERS, *Principles of Solidification* (Krieger, New York, 1977).
13. F. FURTADO, J. GLIMM *et al.*, "Front Tracking and the Interaction of Nonlinear Hyperbolic Waves," Proc. US–ROC Joint Symposium (1988).